

Discovery of a dwarf planet candidate in an extremely wide orbit: 2017 OF201

SIHAO CHENG (程思浩) ,^{1,2} JIAXUAN LI (李嘉轩) ,³ AND ERITAS YANG (杨晴) ,³¹*Institute for Advanced Study, Princeton, NJ 08540, USA*²*Perimeter Institute for Theoretical Physics, Waterloo, N2L 2Y5, ON, Canada*³*Department of Astrophysical Sciences, 4 Ivy Lane, Princeton University, Princeton, NJ 08540, USA*

Submitted to ApJL

Abstract

We report the discovery of a dwarf planet candidate, 2017 OF201, currently located at a distance of 90 au. Its orbit is extremely wide and extends to the inner Oort cloud, with a semi-major axis of 830 au and a perihelion of 45 au, precisely determined from 24 observations over 20 years. Assuming a typical albedo of 0.13, we estimate a diameter \sim 700 km, making it the second-largest known object in this dynamical population and a dwarf planet candidate with the widest orbit. Its high eccentricity suggests that an unseen population of similar objects would total \sim 1% of Earth’s mass. Notably, the longitude of perihelion of 2017 OF201 lies outside the clustering observed in extreme trans-Neptunian objects, posing a challenge to the proposed dynamical evidence for the hypothetical Planet Nine.

Keywords: Solar system (1528) – Trans-Neptunian objects (1705) – Detached objects (376) – Dwarf planets (419) – Scattered disk objects (1430) – Solar system planets (1260)

1. INTRODUCTION

While the asteroid belt contains only less than 10^{-3} of Earth’s mass (M_{\oplus}), the Kuiper Belt harbors fifty times more material (Pitjeva & Pitjev 2018). In the vast region beyond, even greater mass is believed to reside in the scattering disk and Oort Cloud, likely totaling several M_{\oplus} (Gladman & Volk 2021). These distant reservoirs of comets, minor planets, dwarf planets, and possibly undetected massive planets hold essential clues to the formation and evolution history of the solar system. Three decades ago, the first trans-Neptunian objects (TNOs) beyond Pluto was discovered (Jewitt & Luu 1993). Since then, thousands more have been identified⁴ through various surveys, revealing a remarkable richness of this population.

However, the census of TNOs is far from complete in regions beyond about 60 au or at high ecliptic latitudes, even for large objects such as those qualifying as dwarf planets. Due to the challenging scaling relation that the brightness of reflected light drops steeply with distance as r^{-4} , dedicated solar-system surveys are usually either wide (covering \sim 10,000 deg 2) but shallower (e.g., Tru-

jillo & Brown 2003; Schwamb et al. 2010), or deeper but more focused on the ecliptic plane (covering hundreds to a few thousand deg 2 , e.g., Elliot et al. 2005; Petit et al. 2011; Bannister et al. 2018; Sheppard & Trujillo 2016; Sheppard et al. 2019).

Fortunately, recent cosmological imaging surveys, though not dedicated to solar-system science, offer a promising solution to this limitation. With wide sky coverage, deep photometry, and multiple epochs, those surveys are well-suited for detections of faint solar system objects. A prime example is the Dark Energy Survey (DES; Dark Energy Survey Collaboration et al. 2016), whose main scientific goal lies in weak lensing cosmology but has led to the discovery of more than 800 TNOs (Bernardinelli et al. 2022).

In this letter, we report the discovery of a large TNO, 2017 OF201⁵, out of a systematic search in another extra-galactic survey similar to DES but not searched before. This object is likely large enough to qualify as a dwarf planet, and its extremely wide orbit extends to the inner Oort cloud. We also discuss its migration history and interesting implications for the Planet Nine / Planet X hypothesis (Batygin & Brown 2016).

Corresponding author: Sihao Cheng

Email: scheng@ias.edu, jiaxuanli@princeton.edu, eritas.yang@princeton.edu ⁵ <https://www.minorplanetcenter.net/mpec/K25/K25K47.html>⁴ <https://www.minorplanetcenter.net/iau/lists/TNOs.html>

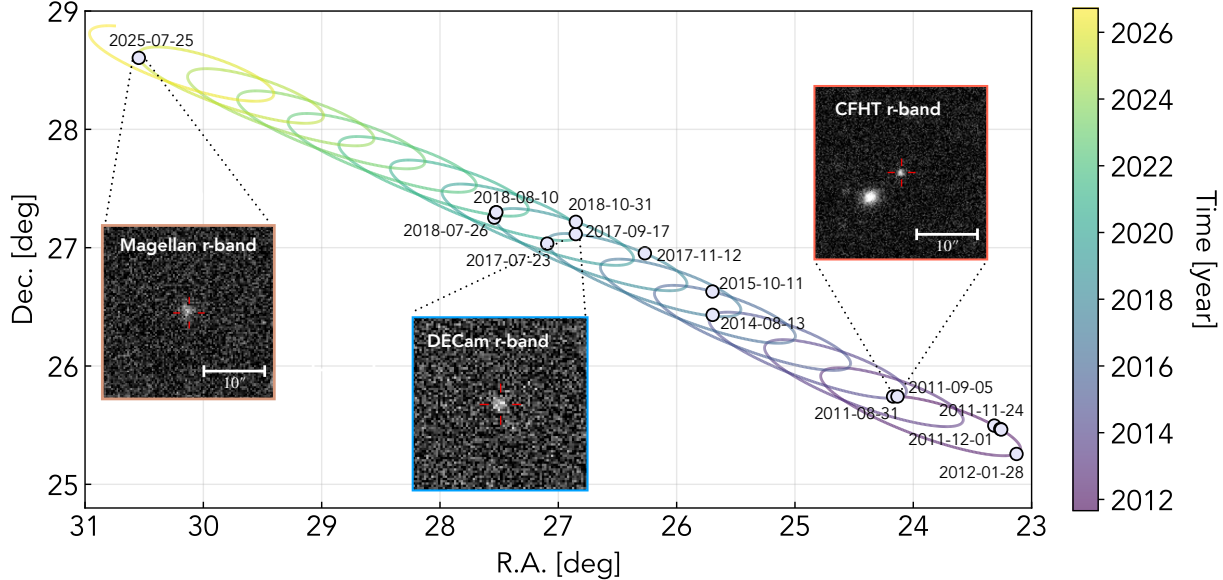


Figure 1. Trajectory of 2017 OF201 on the sky from 2011 to 2025, which is a combination of parallax (elliptic) and proper motion (straight) components. Individual detections from 16 nights are shown with the predicted trajectory based on the best-fit orbit, with a small residue of 0.13 (DECam) and 0.03 (CFHT) arcsec in each component, consistent with their astrometric error. The insets show example images from Magellan, DECam, and CFHT.

2. DISCOVERY

We performed a systematic search for moving objects in the archival data of the Dark Energy Camera Legacy Survey (DECaLS; Dey et al. 2019)⁶. It uses the Dark Energy Camera (DECam) on the 4-meter Blanco telescope (Flaugher et al. 2015), the same facility as DES, and its sky coverage is about two times larger than DES (declination between -15° and $+32^{\circ}$). This dataset has not been searched for TNOs with its full potential, due to its sparse and irregular epoch sampling, which may separate by months to years.

Our search algorithm is similar to Bernardinelli et al. (2020a, 2022), but optimized for the sparse epoch sampling of DECaLS. Details of the algorithm will be described in a future paper. So far, 2017 OF201 is the most interesting object found in our search, with the largest distance and widest orbit.

After identifying 10 detections in three bands (g, r, z) in DECam data between 2014 and 2018, it became clear that they correspond to a single moving object with an extremely wide orbit. With an apparent magnitude $r \sim 22.6$ mag at 85 au away, 2017 OF201 has the second brightest absolute magnitude among 442 known TNOs with wide orbits ($a > 80$ au) in the JPL Small-Body Database⁷.

To further improve the orbital and photometric fitting, we used the ephemeris derived from the DECam detections to quickly search in other data archives. Following suggestions from Mike Alexandersen through a private communication, we found 9 additional r -band images taken in 2011 and 2012 with the 3.6 m Canada–France–Hawaii Telescope (CFHT), where 2017 OF201 is located exactly at the predicted positions⁸. The search was performed using the Solar System Object Image Search (SSOIS) tool⁹ (Gwyn et al. 2012). We also searched the data archive of the Subaru and Gemini-North telescope but unfortunately found no coverage.

After our announcement of 2017 OF201, an amateur astronomer, Sam Deen, found two detections in the Sloan Digital Sky Survey (SDSS; York et al. 2000)¹⁰, taken as early as 2004 and 2009.¹¹ Together with our follow-up observations taken with the 6.5 m Magellan telescope on July 25, 2025, the observational arc has accumulated to 20 years with 24 observations. This unusually long baseline allows us to precisely determine its orbit right after the discovery.

⁸ Taken for a TNO project by Alexandersen et al. (2016). It is a pity that their team missed the discovery of 2017 OF201.

⁹ <https://www.cadc.hia.nrc.gc.ca/en/ssois/>

¹⁰ <http://www.sdss.org/>

¹¹ In SDSS’s object catalog, these two detections have object IDs 1237666274738438899 and 1237680073395798979, misclassified as a star and a galaxy, respectively.

⁶ <https://www.legacysurvey.org/decamls/>

⁷ https://ssd.jpl.nasa.gov/tools/sbdb_query.html

Table 1. Barycentric orbital elements and photometric information of 2017 OF201.

Parameters	Value
a (au)	830.1 ± 0.8
e	0.94589 ± 0.00005
i (deg)	16.20508 ± 0.00006
Ω (deg)	328.5914 ± 0.0004
ω (deg)	337.7290 ± 0.0012
ϖ (deg)	306.3204 ± 0.0013
perihelion q (au)	44.9189 ± 0.0012
aphelion Q (au)	1615.2 ± 1.5
period (yrs)	23900 ± 30
arc length	7612 days (20.84 years)
reference epoch t_0 (MJD)	60881.5 (2025-07-25)
mean anomaly M at t_0	1.4271 ± 0.0019
distance at t_0 (au)	90.7
radial velocity at t_0 (au/yr)	0.64
V mag at t_0	23.3
H_g	4.10 ± 0.09
H_r	3.33 ± 0.05
H_i	2.77 ± 0.10
H_z	2.47 ± 0.10
H_V	3.72 ± 0.09
$g - r$	0.77 ± 0.08
$r - i$	0.56 ± 0.07
$B - V$	0.96 ± 0.09

3. PROPERTIES OF 2017 OF201

Table 1 gives a summary of properties of 2017 OF201 derived from astrometric and photometric measurements of the 22 detection images (Appendix A) and information read directly from SDSS’s catalog.

Figure 1 shows the detections and best-fit orbit of 2017 OF201. It is moving quickly away from us, resulting in a parallax shrink by 15% over 20 years. This significant parallax evolution enables a precise determination of radial velocity – the most uncertain element to measure for TNOs.

The last time 2017 OF201 passed close to us was in November of 1930, and it will come back again in about 25,000 years. Interestingly, this last perihelion was in the same year of Pluto’s discovery (Feb 1930), when 2017 OF201 reached its maximum brightness of $V = 20.2$ mag, about 4 magnitudes fainter than Pluto. Coincidentally, it was also in the same year of the establishment of the Institute for Advanced Study, where the first author of this paper is based.

3.1. Orbit

The orbit of 2017 OF201 is determined using the online version of the `Find_Orb` software¹², which implements a least-squares fitting of the orbital elements to the astrometric measurements of the 24 detections. Thanks to the very long observation arc from 2004 to 2025, the orbit of 2017 OF201 is precisely determined, with the semi-major axis determined to 0.1% precision ($a = 830 \pm 1$ au), revealing an undoubtedly wide orbit with moderate perihelion distance ($q = 44.9$ au) and low inclination ($i = 16.2^\circ$).

Figure 2 shows a comparison between orbits of 2017 OF201 and some other TNOs with extremely wide and eccentric orbits (termed “extreme TNOs”). With such a large aphelion distance (~ 1600 au), the Galactic tide may affect the orbital evolution, placing 2017 OF201 at the boundary between the scattering disk and inner Oort cloud. We shall discuss its dynamical history in Section 4.1.

Another notable characteristic of 2017 OF201’s orbit is its longitude of perihelion $\varpi = 306^\circ$, an outlier to the apparent clustering around $\varpi \approx 60^\circ$ claimed among other extreme TNOs (Figure 2, right panel). First noticed by Trujillo & Sheppard (2014), the clustering has been suggested as evidence for an undetected Planet Nine (also known as Planet X) at several hundred au (e.g., Trujillo & Sheppard 2014; Brown & Batygin 2016; Batygin & Brown 2016; Sheppard et al. 2019; Siraj et al. 2025). We shall discuss the implications of 2017 OF201’s orbit to Planet Nine in Section 4.3.

3.2. Color and variability

2017 OF201 has a color index of $g-r = 0.77 \pm 0.08$ mag, which is much redder than the Sun (0.44; Willmer 2018) and is consistent with other TNOs with scattering-disk and detached orbits (Sheppard 2010; Ofek 2012). Though it is on the red side of the distribution, it is not yet as red as Sedna, which has $B-V = 1.24$. Given the precision and time sampling of the DECam and CFHT data, we do not detect any variability over 0.1 mag, indicating that the shape of 2017 OF201 is likely close to spherical. Deeper imaging with higher cadence is still needed to probe the short-time variability due to rotation or satellite transit.

3.3. Size and mass estimate

We estimate the size of 2017 OF201 based on its observed brightness, distance, and an assumed albedo. We first obtain the V -band absolute magnitude $H_V = 3.7$

¹² <https://www.projectpluto.com/fo.htm>

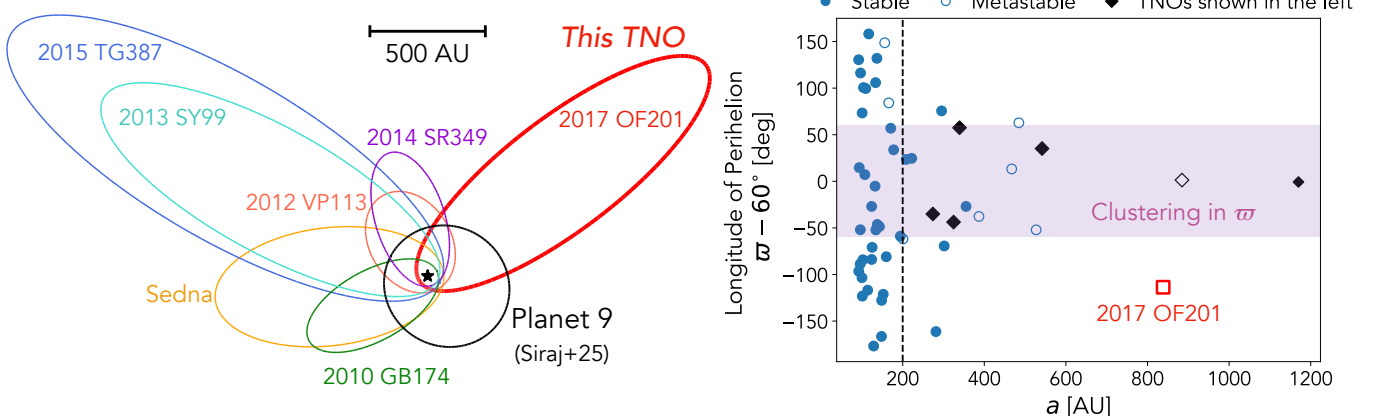


Figure 2. *Left:* Plan view of the orbits of TNOs with extremely wide orbits. The newly discovered 2017 OF201, highlighted in red, is an outlier to the apsidal clustering of the others. For reference, the most probable orbit of Planet 9 / Planet X from Siraj et al. (2025) is shown in black. *Right:* Distribution of longitude of perihelion ϖ of TNOs from Siraj et al. (2025). The purple shaded region indicates the clustering of ϖ around 60° . Objects with (meta)stable orbits are shown as solid (open) symbols.

using the photometry and best-fit orbit (Appendix B), and then estimate the diameter D through the relation $D = 2 \text{ au} \times 10^{0.2(m_\odot - H)} / \sqrt{\rho}$, where m_\odot is the solar apparent magnitude (Willmer 2018) and ρ the geometric albedo. As both D and ρ are unknown and there is only one observable H , ones needs an additional assumption to solve D . One way is the use the observed tight correlation between D and ρ of scattering disk objects (Gerdes et al. 2017; Müller et al. 2020)¹³. We find an estimate of $\rho_V=0.13$ and $D=700$ km fits well both the correlation and observations. This estimate is further validated by comparing it with other TNOs with similar H , such as 2014 UZ224 (Gerdes et al. 2017), which has an albedo of 0.13 ± 0.04 and diameter of 630 ± 70 km measured from thermal emission. Our size estimate of 2017 OF201 indicates that 2017 OF201 is highly likely large enough to achieve hydrostatic equilibrium (e.g. Durham et al. 1997; Tancredi & Favre 2008) and thus qualifies as a dwarf planet.¹⁴

Future observations of thermal emission from ALMA will allow for simultaneous determination of size and albedo without the need to rely on the assumed correlation (e.g., Gerdes et al. 2017). Occultation is another way to directly measure size (e.g., Rommel et al. 2020),

¹³ Also see the first figure in <https://www.johnstonsarchive.net/astro/tnodiam.html>. The physical origin of this relation is that larger objects have dense enough atmospheres that may freeze and form reflecting ice.

¹⁴ As argued by Mike Brown (<https://web.gps.caltech.edu/~mbrown/dps.html>), an icy body larger than 600 km in diameter is “highly likely” a dwarf planet. For reference, the smallest icy body known to be nearly round and thus in hydrostatic equilibrium is Saturn’s satellite Mimas, which has a diameter of about 400 km.

but the next possible occultation event for stars brighter than 21 mag will be in 4 years (Nov 27 2029, 19-mag star), according to the current orbital fitting.

The discovery of such a large object with high eccentricity has interesting implications for the population of objects in trans-Neptunian space. Throughout the orbit, 2017 OF201 is only close enough to be detectable in DECaLS for $\sim 0.5\%$ of the period, which suggests that a substantial population of about 200 similar objects – with large sizes, wide orbits, and high eccentricities – should exist but are just too difficult to detect due to their large distance.

The mass of 2017 OF201 is estimated to be 3×10^{20} kg = $1/20,000 M_\oplus$, when assuming a typical density of 1.7 g cm^{-3} according to the NASA Planetary Data System¹⁵ and a diameter of 700 km. Therefore, the population of 2017 OF201-like objects would add up to order of $1\% M_\oplus$ (about the Moon’s mass). For comparison, the total mass of the classical Kuiper belt is estimated to be 1–2% M_\oplus using object counting and dynamical estimates (e.g. Bernstein et al. 2004; Fraser et al. 2014; Pitjeva & Pitjev 2018; Petit et al. 2023; Bernardinelli et al. 2025), and that of the scattering disk is 1–10% M_\oplus (Gladman et al. 2008; Volk & Malhotra 2008). Therefore, discovery of large TNOs with extremely elongated orbits such as 2017 OF201 and Sedna (Brown et al. 2004) reveals a significant amount of mass in the outer solar system.

¹⁵ <https://sbn.psi.edu/pds/resource/tnocenalb.html> and reference therein.

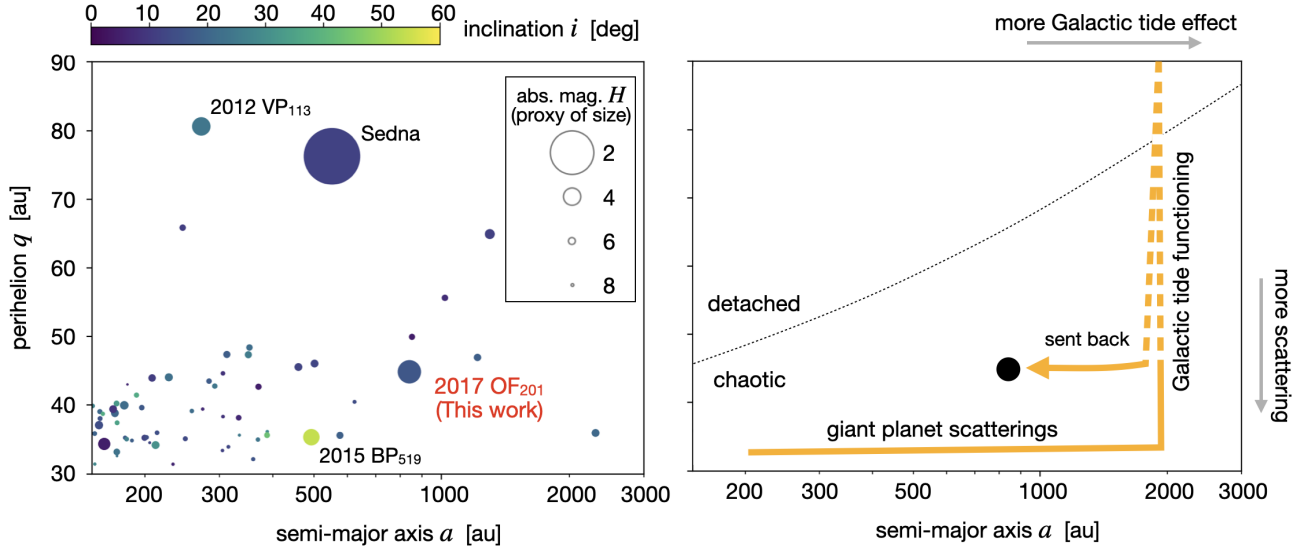


Figure 3. *Left:* TNOs with wide orbits ($a > 150$ au). 2017 OF201 is the second brightest in this population and has the widest orbit among all dwarf planet candidates. *Right:* Schematic of a possible migration pathway for 2017 OF201. The object may first have been scattered to a large a while maintaining a low q and then galactic tidal torques slowly increase q , detaching the orbit from Neptune.

4. ORBITAL DYNAMICS

4.1. Possible origin

The semi-major axis of 2017 OF201 evolves through chaotic diffusion driven by interactions with Neptune. However, the diffusion timescale T increases steeply with perihelion distance. Following Hadden & Tremaine (2024), it is approximately

$$T \approx 0.2 \text{ Myr} \times \exp \left[7.4 \left(\frac{q}{a_N} \right) \right] \approx 10^{10} \text{ yr}, \quad (1)$$

where a_N is the semi-major axis of Neptune and q is the perihelion distance of 2017 OF201. This implies that 2017 OF201 cannot reach its current large semi-major axis through perturbations from Neptune alone, given the age of the solar system. Instead, its high- q , large- a orbit likely reflects the influence of external torques from stellar encounters or the Galactic tide, which act during or after an initial scattering event (Duncan et al. 1987; Bannister et al. 2017; Gladman & Volk 2021; Batygin et al. 2021).

2017 OF201 may have first been scattered outward by Neptune while retaining a low perihelion. Once at large a , the Galactic tide becomes dynamically important, gradually increasing q and detaching the orbit from Neptune. As the perihelion rises into a region where planetary perturbations are weak, the object undergoes slow angular momentum oscillation and reaches a configuration like that observed today (Figure 3). Or, alternatively, a passing star in the birth cluster of the Sun may provide the torque to raise q (Nesvorný et al. 2023).

4.2. Long-term stability

We investigate the long-term dynamical stability of 2017 OF201 using direct N -body integrations with the `ias15` integrator (Rein & Spiegel 2015) in `REBOUND`¹⁶ (Rein & Liu 2012). Because scattering of distant objects is primarily driven by Uranus and Neptune (Batygin & Brown 2016; Gerdes et al. 2017), we explicitly include these planets in our simulations. Jupiter and Saturn are incorporated through a static solar quadrupole moment (J_2), which efficiently captures their secular influence.¹⁷ Given 2017 OF201's large aphelion distance (~ 1600 au), we additionally include the vertical component of the Galactic tide (Levison et al. 2001) using the `add_force` module in `REBOUNDx`¹⁸ (Tamayo et al. 2020).

We draw 100 realizations of 2017 OF201's orbits from a multivariate normal distribution based on the best-fit orbital parameters and their uncertainties, and integrate each system for 4 Gyr. At the end of the integrations, 2017 OF201 remains bound in more than 80% of realizations, yet in roughly half of cases its semi-major axis varies by a factor of ≥ 2 . Following the criterion of Batygin & Brown (2021), we therefore classify 2017 OF201 as metastable.

¹⁶ <https://rebound.readthedocs.io/>

¹⁷ For validation, we also performed computationally intensive integrations that directly included Jupiter and Saturn. The outcomes were qualitatively consistent with our simplified model.

¹⁸ <https://reboundx.readthedocs.io/>

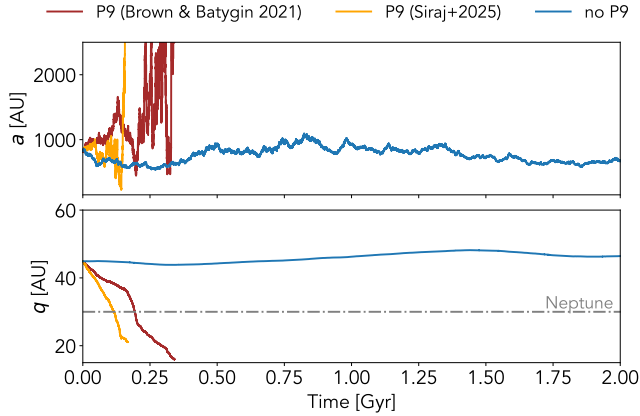


Figure 4. Typical clones of dynamical evolution simulation of 2017 OF201, with and without P9. In the absence of P9, 2017 OF201 remains stable over 4 Gyr under the influence of the known giant planets and the Galactic tide (the x-axis is truncated for clarity). By contrast, when P9 is included, 2017 OF201 undergoes close encounters with Neptune and is ejected from the Solar System within ~ 0.3 Gyr.

4.3. Implications for the hypothetical Planet Nine

As shown in Figure 2, the longitude of perihelion of 2017 OF201, $\varpi = 306^\circ$, lies well outside the clustering region near $\varpi \approx 60^\circ$ observed among other extreme TNOs. This discrepancy raises the question of whether 2017 OF201 is dynamically compatible with the Planet Nine (P9) hypothesis, which posits that a distant massive planet shepherds TNOs into aligned orbital configurations.

Brown & Batygin (2021) inferred a candidate P9 with mass $m_p = 6.2 M_\oplus$, semimajor axis $a_p = 382.4$ au, eccentricity $e_p = 0.20$, inclination $i_p = 15.6^\circ$, and longitude of perihelion $\varpi_p = 246.7^\circ$. More recently, Siraj et al. (2025) derived an updated configuration that simultaneously reproduces the observed orbital clustering and preserves the stability of already stable TNOs, yielding $m_p = 4.1 M_\oplus$, $a_p = 296$ au, $e_p = 0.339$, $i_p = 4.27^\circ$, and $\varpi_p = 242^\circ$.

To evaluate the influence of a putative P9 on 2017 OF201, we performed forward N -body integrations including P9 with each of the parameter sets described above, and compared the results against a control case without P9. For each configuration, we fixed all orbital elements of P9 to their mean values and sampled 100 values of the mean anomaly of P9 uniformly across $[0, 2\pi]$, integrating the systems for 4 Gyr. With the parameters proposed by Brown & Batygin (2021), 56% of realizations resulted in ejection of 2017 OF201, whereas the updated parameters from Siraj et al. (2025) produced a 64% ejection fraction. The corresponding mean ejection

timescales are 0.31 and 0.25 Gyr, respectively. Figure 4 shows typical clones of the simulation result.

These results suggest that the orbit of 2017 OF201 is difficult to reconcile with the specific P9 configurations from Brown & Batygin (2021) and Siraj et al. (2025). Therefore, 2017 OF201 offers an additional challenge to the P9 hypothesis, complementing other challenges such as observational selection effects and questions regarding the statistical significance of the reported clustering (Shankman et al. 2017; Bernardinelli et al. 2020b; Napier et al. 2021).

5. CONCLUSION

We report the discovery of a large, exotic trans-Neptunian dwarf planet candidate, 2017 OF201, from the archival data of DECaLS. It is currently located at a distance of 90 au. When assuming a typical albedo of 0.13, its diameter is estimated to be 700 km, large enough to qualify as a dwarf planet.

Its orbit is extremely wide and eccentric ($a = 830$ au, $q = 44.9$ au, $i = 16.2^\circ$), influenced by both Neptune's scattering and the Galactic tide at Gyr timescale, therefore representing an overlap between the scattering disk and the inner Oort cloud.

The probability for 2017 OF201 to be close enough and detectable is only 0.5% given its wide and eccentric orbit. Therefore, there should exist a population of hundreds of 2017 OF201-like objects in the outer solar system, totaling 1% of Earth's mass, a significant fraction of the scattering disk.

The orbit of 2017 OF201 also poses a challenge to the Planet Nine (P9) hypothesis. Previous discoveries of extreme TNOs reveal an apparent clustering in longitude of perihelion near $\varpi \approx 60^\circ$, motivating the idea that an undetected planet shepherds their orbits. By contrast, 2017 OF201, with $\varpi = 306^\circ$, lies well outside this clustering region (Figure 2) and appears dynamically inconsistent with confinement by P9. Our N -body simulations indicate that the inclusion of such a planet leads to ejection of 2017 OF201 in $\sim 60\%$ of realizations, with a mean timescale of ~ 0.3 Gyr (Figure 4). Further investigation will be necessary to assess whether this outcome robustly excludes the P9 hypothesis.

Facilities: Blanco (DECam), CFHT (MegaCam), Magellan

Software: astropy (Astropy Collaboration et al. 2013), matplotlib (Hunter 2007), scipy (Jones et al. 2001), SExtractor (Bertin & Arnouts 1996), PSFEx (Bertin 2011), SCAMP (Bertin 2006), astrometry.net (Lang et al. 2010).

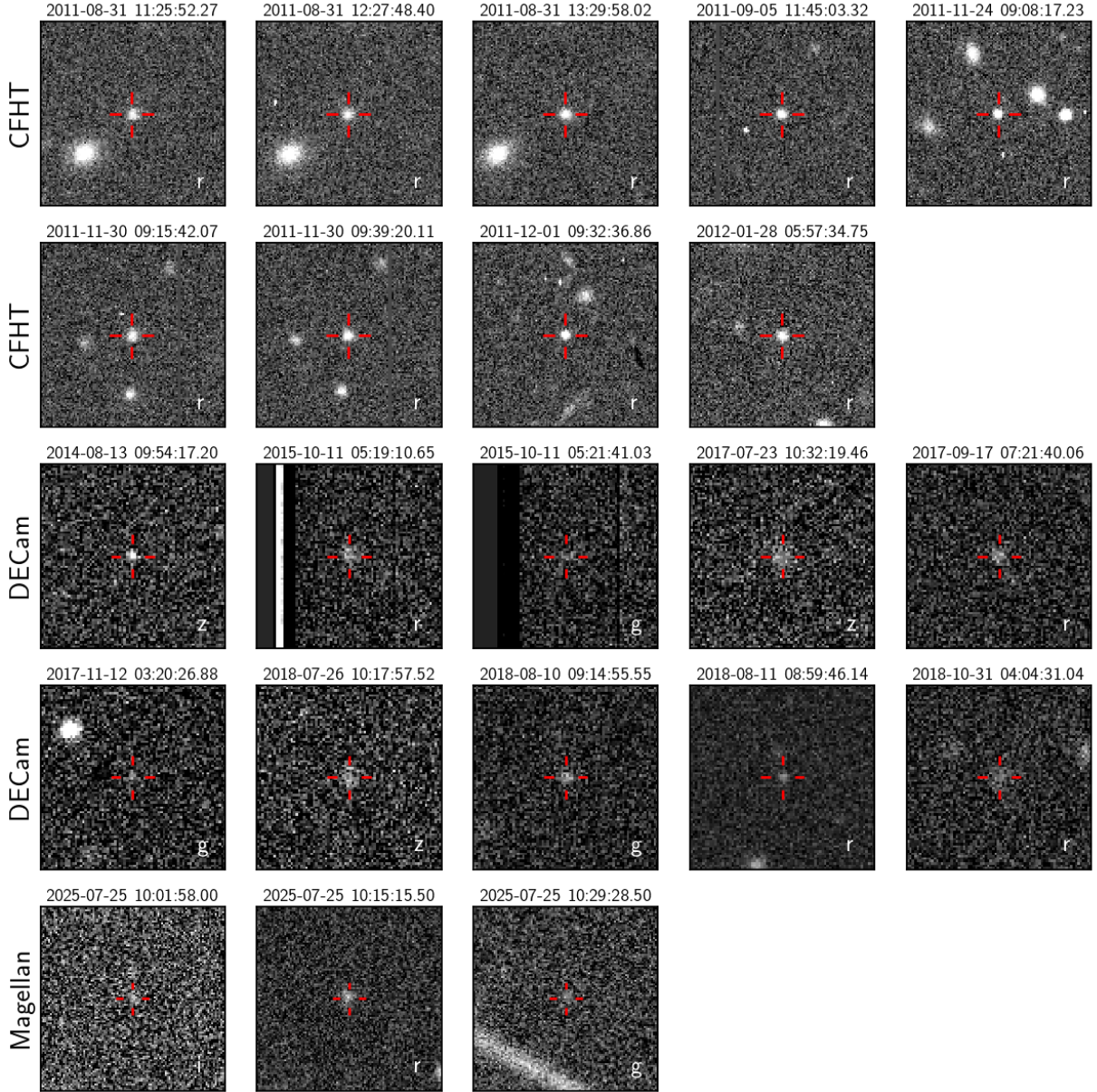


Figure 5. Cutout images of all 22 detections from CFHT, DECam, and Magellan. Each image is 20 arcsec on a side. The detection time corresponds to the middle of each exposure. CFHT data are deeper and have a much better seeing than the DECam data. The detection spans a long time baseline from Aug 2011 to Jul 2025, enabling precise determination of its orbit.

APPENDIX

A. ASTROMETRY AND PHOTOMETRY

We perform astrometric and photometric measurements of the object using the CFHT/MegaCam, DECam, and Magellan imaging data. Cutouts of those images with 2017 OF201 centered are shown in Figure 5.

For the detections in CFHT, we retrieve the single-epoch images from the Canada-France-Hawaii Telescope (CFHT)/MegaCam data archive¹⁹. These images are all in the *r*-band with 0.5–0.9 arcsec seeing. The instrument

¹⁹ <https://www.cadc-ccda.hia-iha.nrc-cnrc.gc.ca/>

Table 2. Archival and follow-up observations of 2017 OF201. The codes in parentheses are station codes of the observatory from the minor planet center. Note that the photometry reported here are measured in the native filter systems.

observation time	R.A.	rms	Dec.	rms	magnitude	band	seeing	expo.	α	$H(\alpha)$
UTC	deg	”	deg	”			”	s	deg	
SDSS (645)										
2004-09-21 06:02:01.31	20.4237305	0.08	+23.8643205	0.08	22.42 \pm 0.12	<i>r</i>	1.0	54	0.40	3.54
					23.16 \pm 0.42	<i>u</i>				4.29
					23.22 \pm 0.16	<i>g</i>				4.35
					21.58 \pm 0.09	<i>i</i>				2.71
					21.24 \pm 0.25	<i>z</i>				2.37
2009-09-26 10:49:07.74	22.9414929	0.10	+25.2131626	0.08	22.47 \pm 0.12	<i>r</i>	0.9	54	0.37	3.43
					23.52 \pm 0.84	<i>u</i>				4.48
					23.22 \pm 0.17	<i>g</i>				4.18
					22.20 \pm 0.14	<i>i</i>				3.16
					21.96 \pm 0.41	<i>z</i>				2.92
CFHT (T14)										
2011-08-31 11:25:52.27	24.1672646	0.030	+25.7422073	0.030	22.659 \pm 0.038	<i>r</i>	0.9	320	0.59	3.543
2011-08-31 12:27:48.41	24.1669749	0.026	+25.7422438	0.025	22.604 \pm 0.035	<i>r</i>	0.9	320	0.59	3.488
2011-08-31 13:29:58.02	24.1666503	0.022	+25.7422514	0.022	22.634 \pm 0.032	<i>r</i>	0.8	320	0.59	3.518
2011-09-05 11:45:03.32	24.1300816	0.020	+25.7423370	0.018	22.582 \pm 0.029	<i>r</i>	0.7	320	0.55	3.467
2011-11-24 09:08:17.23	23.3120374	0.013	+25.4947651	0.013	22.588 \pm 0.022	<i>r</i>	0.5	320	0.38	3.471
2011-11-30 09:15:42.08	23.2618590	0.027	+25.4661271	0.026	22.610 \pm 0.036	<i>r</i>	0.9	320	0.44	3.490
2011-11-30 09:39:20.11	23.2617232	0.020	+25.4660430	0.020	22.610 \pm 0.030	<i>r</i>	0.7	320	0.44	3.490
2011-12-01 09:32:36.86	23.2539409	0.013	+25.4613167	0.013	22.632 \pm 0.022	<i>r</i>	0.5	320	0.45	3.512
2012-01-28 05:57:34.76	23.1285940	0.027	+25.2561656	0.024	22.656 \pm 0.038	<i>r</i>	0.8	384	0.68	3.508
DECam (W84)										
2015-10-11 05:21:41.03	25.694931	0.15	+26.629005	0.18	23.32 \pm 0.22	<i>g</i>	1.5	125	0.25	4.08
2017-11-12 03:20:26.88	26.267165	0.19	+26.952323	0.22	24.32 \pm 0.26	<i>g</i>	1.3	200	0.24	5.01
2018-08-10 09:14:55.55	27.525852	0.07	+27.298418	0.08	23.49 \pm 0.10	<i>g</i>	1.3	168	0.66	4.14
2015-10-11 05:19:10.66	25.694897	0.10	+26.629028	0.10	22.54 \pm 0.10	<i>r</i>	1.3	119	0.25	3.23
2017-09-17 07:21:40.06	26.850032	0.06	+27.114610	0.07	22.71 \pm 0.09	<i>r</i>	1.2	110	0.46	3.40
2018-08-11 08:59:46.14	27.523248	0.05	+27.300693	0.05	22.62 \pm 0.09	<i>r</i>	0.9	40	0.66	3.27
2018-10-31 04:04:31.05	26.850075	0.11	+27.217787	0.12	22.65 \pm 0.11	<i>r</i>	1.8	118	0.18	3.31
2014-08-13 09:54:17.21	25.694468	0.05	+26.432920	0.05	21.79 \pm 0.09	<i>z</i>	0.8	146	0.67	2.57
2017-07-23 10:32:19.46	27.094235	0.11	+27.035966	0.09	21.77 \pm 0.10	<i>z</i>	1.8	250	0.68	2.44
2018-07-26 10:17:57.53	27.541774	0.11	+27.255624	0.10	22.02 \pm 0.12	<i>z</i>	1.4	229	0.67	2.67
Magellan (304)										
2025-07-25 10:01:58.00	30.547527	0.10	+28.609305	0.10	22.69 \pm 0.18	<i>i</i>	1.0	600	0.64	3.11
2025-07-25 10:15:15.50	30.547569	0.05	+28.609342	0.05	23.10 \pm 0.06	<i>r</i>	1.1	600	0.64	3.52
2025-07-25 10:29:28.50	30.547500	0.12	+28.609326	0.12	23.79 \pm 0.17	<i>g</i>	1.2	700	0.64	4.21

signatures (bias, dark, and flat) have been removed in these images, but they do not yet have astrometric solutions and photometric calibrations. We implement a two-step astrometric calibration process: first obtaining an initial solution using `astrometry.net` (Lang et al. 2010), followed by fine-tuning against Gaia DR3 reference stars (Gaia Collaboration et al. 2021) using `SCAMP` (Bertin 2006). This procedure yields a final astrometric solution with an average positional uncertainty of 0.1''. For photometric calibration, we first remove the sky background using `SEExtractor` (Bertin & Arnouts 1996) with a mesh size of 60''. We then construct a point spread function (PSF) model using `PSFEx` (Bertin

2011) from non-saturated point sources in each image, and perform PSF-fitting photometry using **SExtractor**. The photometric zeropoint is thus determined by comparing the instrumental magnitudes of non-saturated stars with their Pan-STARRS1 PSF magnitudes. Our object has an average r -band magnitude of $r = 22.61$ mag in the CFHT data from 2011 to 2012.

The DECam single-epoch images are downloaded from the Legacy Surveys²⁰, which are reduced using the DECam Community Pipeline²¹. These images are photometrically calibrated using Pan-STARRS1 (Chambers et al. 2016) and have a preliminary astrometric solution. To ensure consistency with our CFHT analysis, we refine the astrometric calibration using **SCAMP** against the Gaia DR3 catalog. Similar to the CFHT data above, for each DECam image, we subtract the sky background with a mesh size of $60''$, generate the PSF model, and perform PSF-fitting photometry. The resulting photometry have higher uncertainties since the DECam images are shallower and have poorer seeing conditions (0.8–2.0 arcsec) than the CFHT images.

We also include the SDSS detections on 2004 and 2009 for our orbital fitting. In fact, those detections are listed as two objects in SDSS’s catalog, with object ID 1237666274738438899 and 1237680073395798979, and misclassified as a star and a galaxy. This is because SDSS has only single-epoch observations on most part of its coverage and therefore cannot distinguish slowly-moving objects from static ones. As the SDSS catalog has a high accuracy of astrometric calibration with a systematic error below $0.03''$ (Pier et al. 2003), we directly use the astrometry (r -band) and photometry values in the catalog (Fukugita et al. 1996; Gunn et al. 1998; Lupton et al. 1999). Note that when considering photometry, one should use columns of **psfMag** instead of the default magnitude in the catalog due to the mis-classification of object type.

B. ABSOLUTE MAGNITUDE

The phase angle α and reduced magnitude $H(\alpha)$ of each observations of 2017 OF201 are listed in table 2, using the best-fit orbit. The absolute magnitude H is defined as the reduced magnitude $H(\alpha) = m - 5 \lg(r\Delta)$ when $\alpha = 0$, where α is the phase angle, m is the apparent magnitude, r is the heliocentric distance, Δ is the geocentric distance. The phase curve $H(\alpha)$ reveals surface reflective properties of the object. Due to the limited range of phase angle of TNOs (0–2°), phase curves are usually fit with a linear function $H(\alpha) = H + \beta\alpha$ (e.g. Rabinowitz et al. 2007).

For 2017 OF201, only the r -band has good enough photometry to fit simultaneously H and β , which leads to $H_r = 3.33 \pm 0.05$ and $\beta_r = 0.12 \pm 0.11$ per degree. The slope β is consistent with the average value of 0.15 measured from other TNOs (e.g. Sheppard & Jewitt 2002; Rabinowitz et al. 2007), though the uncertainty is yet to be improved. The absolute magnitudes in other bands listed in table 2 are obtained by a least square fitting with the slope fixed to $\beta = 0.12 \pm 0.11$ per degree. Before fitting, all observed magnitudes from SDSS, CFHT, and Magellan (McLeod et al. 2015) have been converted into the DECam system²².

ACKNOWLEDGMENTS

We thank Scott Tremaine, Yubo Su, Daniel Tamayo, Amir Siraj, Konstantin Batygin, Mike Brown, Yukun Huang, Yen-Ting Lin, Sam Hadden, Kat Volk, and Marla Geha for useful discussions and suggestions. We thank Mike Alexandersen at the Minor Planet Center for suggesting a follow-up search in the CFHT archive. SC thanks Siyu Yao for her constant inspiration and encouragement. SC acknowledges the support of the Martin A. and Helen Chooljian Member Fund and the Fund for Natural Sciences at the Institute for Advanced Study.

This work is partly based on observations of the Legacy Surveys. The Legacy Surveys consist of three individual and complementary projects: the Dark Energy Camera Legacy Survey (DECaLS; Proposal ID #2014B-0404; PIs: David Schlegel and Arjun Dey), the Beijing-Arizona Sky Survey (BASS; NOAO Prop. ID #2015A-0801; PIs: Zhou Xu and Xiaohui Fan), and the Mayall z-band Legacy Survey (MzLS; Prop. ID #2016A-0453; PI: Arjun Dey). DECaLS, BASS and MzLS together include data obtained, respectively, at the Blanco telescope, Cerro Tololo Inter-American Observatory, NSF’s NOIRLab; the Bok telescope, Steward Observatory, University of Arizona; and the Mayall telescope, Kitt Peak National Observatory, NOIRLab. Pipeline processing and analyses of the data were supported by NOIRLab and the Lawrence Berkeley National Laboratory (LBNL). The Legacy Surveys project is honored to be

²⁰ <https://www.legacysurvey.org/rawdata/>

²¹ <https://noirlab.edu/science/data-services/data-reduction-software/csd-cms-pipelines/pl206>

²² <https://des.ncsa.illinois.edu/releases/dr2/dr2-docs/dr2-transformations>

permitted to conduct astronomical research on Iolkam Du'ag (Kitt Peak), a mountain with particular significance to the Tohono O'odham Nation.

The Legacy Surveys imaging of the DESI footprint is supported by the Director, Office of Science, Office of High Energy Physics of the U.S. Department of Energy under Contract No. DE-AC02-05CH1123, by the National Energy Research Scientific Computing Center, a DOE Office of Science User Facility under the same contract; and by the U.S. National Science Foundation, Division of Astronomical Sciences under Contract No. AST-0950945 to NOAO.

This paper includes data gathered with the 6.5-meter Magellan Telescopes located at Las Campanas Observatory, Chile.

This work is partly based on observations obtained with MegaPrime/MegaCam, a joint project of CFHT and CEA/DAPNIA, at the Canada-France-Hawaii Telescope (CFHT) which is operated by the National Research Council (NRC) of Canada, the Institut National des Sciences de l'Univers of the Centre National de la Recherche Scientifique (CNRS) of France, and the University of Hawaii. The observations at the Canada-France-Hawaii Telescope were performed with care and respect from the summit of Maunakea which is a significant cultural and historic site.

Funding for the SDSS and SDSS-II has been provided by the Alfred P. Sloan Foundation, the Participating Institutions, the National Science Foundation, the U.S. Department of Energy, the National Aeronautics and Space Administration, the Japanese Monbukagakusho, the Max Planck Society, and the Higher Education Funding Council for England. The SDSS Web Site is <http://www.sdss.org/>.

This research used resources of the National Energy Research Scientific Computing Center (NERSC), a Department of Energy Office of Science User Facility using NERSC award HEP-ERCAP0030970.

The authors are pleased to acknowledge that the work reported in this paper was substantially performed using the Princeton Research Computing resources at Princeton University, a consortium of groups led by the Princeton Institute for Computational Science and Engineering (PICSciE) and the Office of Information Technology's Research Computing.

References

Alexandersen, M., Gladman, B., Kavelaars, J. J., et al. 2016, *AJ*, **152**, 111

Astropy Collaboration, Robitaille, T. P., Tollerud, E. J., et al. 2013, *A&A*, **558**, A33

Bannister, M. T., Shankman, C., Volk, K., et al. 2017, *AJ*, **153**, 262

Bannister, M. T., Gladman, B. J., Kavelaars, J. J., et al. 2018, *ApJS*, **236**, 18

Batygin, K., & Brown, M. E. 2016, *AJ*, **151**, 22

—. 2021, *ApJL*, **910**, L20

Batygin, K., Mardling, R. A., & Nesvorný, D. 2021, *ApJ*, **920**, 148

Bernardinelli, P. H., Bernstein, G. M., Sako, M., et al. 2020a, *ApJS*, **247**, 32

—. 2020b, *PSJ*, **1**, 28

—. 2022, *ApJS*, **258**, 41

Bernardinelli, P. H., Bernstein, G. M., Abbott, T. M. C., et al. 2025, *AJ*, **169**, 305

Bernstein, G. M., Trilling, D. E., Allen, R. L., et al. 2004, *AJ*, **128**, 1364

Bertin, E. 2006, in Astronomical Society of the Pacific Conference Series, Vol. **351**, Astronomical Data Analysis Software and Systems XV, ed. C. Gabriel, C. Arviset, D. Ponz, & S. Enrique, 112

Bertin, E. 2011, in Astronomical Society of the Pacific Conference Series, Vol. **442**, Astronomical Data Analysis Software and Systems XX, ed. I. N. Evans, A. Accomazzi, D. J. Mink, & A. H. Rots, 435

Bertin, E., & Arnouts, S. 1996, *A&AS*, **117**, 393

Brown, M. E., & Batygin, K. 2016, *ApJL*, **824**, L23

—. 2021, *AJ*, **162**, 219

Brown, M. E., Trujillo, C., & Rabinowitz, D. 2004, *ApJ*, **617**, 645

Chambers, K. C., Magnier, E. A., Metcalfe, N., et al. 2016, *arXiv e-prints*, arXiv:1612.05560

Dark Energy Survey Collaboration, Abbott, T., Abdalla, F. B., et al. 2016, *MNRAS*, **460**, 1270

Dey, A., Schlegel, D. J., Lang, D., et al. 2019, *AJ*, **157**, 168

Duncan, M., Quinn, T., & Tremaine, S. 1987, *AJ*, **94**, 1330

Durham, W. B., Kirby, S. H., & Stern, L. A. 1997, *J. Geophys. Res.*, **102**, 16293

Elliot, J. L., Kern, S. D., Clancy, K. B., et al. 2005, *AJ*, **129**, 1117

Flaugher, B., Diehl, H. T., Honscheid, K., et al. 2015, *AJ*, **150**, 150

Fraser, W. C., Brown, M. E., Morbidelli, A., Parker, A., & Batygin, K. 2014, *ApJ*, **782**, 100

Fukugita, M., Ichikawa, T., Gunn, J. E., et al. 1996, *AJ*, **111**, 1748

Gaia Collaboration, Brown, A. G. A., Vallenari, A., et al. 2021, *A&A*, **649**, A1

Gerdes, D. W., Sako, M., Hamilton, S., et al. 2017, *ApJL*, **839**, L15

Gladman, B., Marsden, B. G., & Vanlaerhoven, C. 2008, Nomenclature in the Outer Solar System, ed. M. A. Barucci, H. Boehnhardt, D. P. Cruikshank, A. Morbidelli, & R. Dotson, 43

Gladman, B., & Volk, K. 2021, *ARA&A*, **59**, 203

Gunn, J. E., Carr, M., Rockosi, C., et al. 1998, *AJ*, **116**, 3040

Gwyn, S. D. J., Hill, N., & Kavelaars, J. J. 2012, *PASP*, **124**, 579

Hadden, S., & Tremaine, S. 2024, *MNRAS*, **527**, 3054

Hunter, J. D. 2007, *Computing in Science Engineering*, **9**, 90

Jewitt, D., & Luu, J. 1993, *Nature*, **362**, 730

Jones, E., Oliphant, T., Peterson, P., et al. 2001, SciPy: Open source scientific tools for Python

Lang, D., Hogg, D. W., Mierle, K., Blanton, M., & Roweis, S. 2010, *AJ*, **139**, 1782

Levison, H. F., Dones, L., & Duncan, M. J. 2001, *AJ*, **121**, 2253

Lupton, R. H., Gunn, J. E., & Szalay, A. S. 1999, *AJ*, **118**, 1406

McLeod, B., Geary, J., Conroy, M., et al. 2015, *PASP*, **127**, 366

Müller, T., Lellouch, E., & Fornasier, S. 2020, in *The Trans-Neptunian Solar System*, ed. D. Prialnik, M. A. Barucci, & L. Young, 153

Napier, K. J., Gerdes, D. W., Lin, H. W., et al. 2021, *PSJ*, **2**, 59

Nesvorný, D., Bernardinelli, P., Vokrouhlický, D., & Batygin, K. 2023, *Icarus*, **406**, 115738

Ofek, E. O. 2012, *ApJ*, **749**, 10

Petit, J.-M., Gladman, B., Kavelaars, J. J., et al. 2023, *ApJL*, **947**, L4

Petit, J. M., Kavelaars, J. J., Gladman, B. J., et al. 2011, *AJ*, **142**, 131

Pier, J. R., Munn, J. A., Hindsley, R. B., et al. 2003, *AJ*, **125**, 1559

Pitjeva, E. V., & Pitjev, N. P. 2018, *Astronomy Letters*, **44**, 554

Rabinowitz, D. L., Schaefer, B. E., & Tourtellotte, S. W. 2007, *AJ*, **133**, 26

Rein, H., & Liu, S. F. 2012, *A&A*, **537**, A128

Rein, H., & Spiegel, D. S. 2015, *MNRAS*, **446**, 1424

Rommel, F. L., Braga-Ribas, F., Desmars, J., et al. 2020, *A&A*, **644**, A40

Schwamb, M. E., Brown, M. E., Rabinowitz, D. L., & Ragozzine, D. 2010, *ApJ*, **720**, 1691

Shankman, C., Kavelaars, J. J., Bannister, M. T., et al. 2017, *AJ*, **154**, 50

Sheppard, S. S. 2010, *AJ*, **139**, 1394

Sheppard, S. S., & Jewitt, D. C. 2002, in *ESA Special Publication*, Vol. **500**, Asteroids, Comets, and Meteors: ACM 2002, ed. B. Warmbein, 21

Sheppard, S. S., & Trujillo, C. 2016, *AJ*, **152**, 221

Sheppard, S. S., Trujillo, C. A., Tholen, D. J., & Kaib, N. 2019, *AJ*, **157**, 139

Siraj, A., Chyba, C. F., & Tremaine, S. 2025, *ApJ*, **978**, 139

Tamayo, D., Rein, H., Shi, P., & Hernandez, D. M. 2020, *MNRAS*, **491**, 2885

Tancredi, G., & Favre, S. 2008, *Icarus*, **195**, 851

Trujillo, C. A., & Brown, M. E. 2003, *Earth Moon and Planets*, **92**, 99

Trujillo, C. A., & Sheppard, S. S. 2014, *Nature*, **507**, 471

Volk, K., & Malhotra, R. 2008, *ApJ*, **687**, 714

Willmer, C. N. A. 2018, *ApJS*, **236**, 47

York, D. G., Adelman, J., Anderson, Jr., J. E., et al. 2000, *AJ*, **120**, 1579